(Received 1 April 2026, Accepted 6 May 2026, Scheduled 19 May 2026)

A Compact Jeans-Based Patch Antenna for Wearable Applications

Monika Budania*, Bharati Singh, and Vandana Satam

Department of Electronics and Telecommunication Engineering
K. J. Somaiya School of Engineering, Somaiya Vidyavihar University, Vidyanagar, Mumbai, India

ABSTRACT: This study details the design and analysis of a tri-arm-shaped microstrip patch antenna with a partial ground plane, intended for wearable applications. The proposed antenna is designed on a flexible jeans substrate and operates within the Industrial, Scientific, and Medical (ISM) band (2.40–2.48 GHz). It features a low-profile structure with overall dimensions of $40 \times 20 \times 1.2\,\text{mm}^3$, impedance bandwidth of 580 MHz, and radiation efficiency of 82%. Impedance matching and miniaturization were achieved in the design through the use of the stub loading technique. Furthermore, on-body measurements, such as bending and crumpling analyses, demonstrated its robust performance with good return loss values. The Specific Absorption Rate complies with the safety limits, and the proposed conformal antenna is reliable for wearable applications.

1. INTRODUCTION

The art of miniaturization and the rapid boom in wearable technology have led to a surge in the use of wearable devices. Wearable antennas, which are integrated into clothing or embedded in wearable devices, are required for data transmission in wireless-body centric communication (WBCC). WBCC plays a vital role in enhancing the quality of life as it allows early detection of medical conditions and personalized healthcare, in sports and military for tracking, security purposes, etc. [1, 2]. Several challenges are faced when designing a wearable antenna, as it is positioned on the human body, which impacts the antenna's performance metrics, such as gain, bandwidth, efficiency, and radiation characteristics, due to the high dielectric properties of biological tissues. Wearable antennas should be flexible, compact, and sustain performance during movements, including bending and crumpling, while providing comfort to the wearer. Furthermore, the Specific Absorption Rate (SAR), which measures the amount of radiated power absorbed by biological tissues, should be within the standard limits to ensure the safety of individuals [3].

Recently, Metasurfaces (MSs) have gained more attention in wearable antenna design for improving SAR. In [4], the authors used an Artificial Magnetic Conductor (AMC) array to improve gain and reduce the SAR of a Coplanar Waveguide (CPW)-fed triangular antenna. This dual-band antenna achieved an efficiency of 83.56% at 3.5 GHz and 91.2% at 4.8 GHz band. Although the SAR of the antenna was low, the overall structure was bulky and showed poor performance in close proximity to body tissues. It required significant separation from the body (15 mm) along with a large AMC plane ($86 \times 86\,\text{mm}^2$), which compromises the comfort of the wearer in real time. In [5], the authors presented an aperture-coupled broadband antenna using a nonuniform MS operating in the frequency range of 4.72 to 6.19 GHz. The impedance bandwidth obtained was 26.73% with a measured average gain of 7.23 dBi. The utilized MS improved the antenna performance at the cost of higher design complexity. In [6], a textile antenna with an AMC was proposed for the ISM 5.8 GHz band. The impedance bandwidth achieved was 34% with a peak gain of 6.12 dBi, and SAR values were within safety limits. The antenna showed robust performance with respect to structural deformations, such as bending and crumpling. The large and complex AMC unit cell structure ($102 \times 68 \times 3.6\,\text{mm}^3$) presents challenges for integration in compact wearable devices. While the metamaterial structures have improved antenna performance, there is an increase in antenna profile and design complexity. The integration of these surfaces is challenging in real-time wearable applications [7]. In [8], the authors introduced two textile-based wearable antennas on cotton jean material using embroidery technique, operating at 2.4 GHz. The proposed dipole antenna achieved a bandwidth of 130 MHz, gain of 2.3 dB, and efficiency around 95%. The other design proposed was a loop antenna which achieved an impedance bandwidth of 45 MHz and efficiency around 98%. The bending analysis showed minor variations in resonant frequency. The on-body tests were performed, which showed a shift in antenna resonant frequency by 100 MHz. In [9], the authors introduced a dual-band textile Planar Inverted F Antenna (PIFA) with a defected ground plane. The antenna achieved an impedance bandwidth of 35 MHz at the operating frequencies of 433 MHz and 309 MHz at 2.4 GHz. The corresponding radiation efficiencies in free space were 48% and 64%, respectively. However, when measured on the body, the efficiency values were reduced to 7%–13%. The SAR investigations are missing in the study. In [10], the authors presented a compact low-profile antenna by incorporating a Koch fractal geometry along with slits and a Defective Ground Structure (DGS). The triangular patch antenna operated at 2.45 GHz, with an impedance bandwidth of 7.75%, a peak gain of 2.06 dBi, and a radiation efficiency of 75%. However, the antenna exhibits

* Corresponding author: Monika Budania (monika.budania@somaiya.edu).

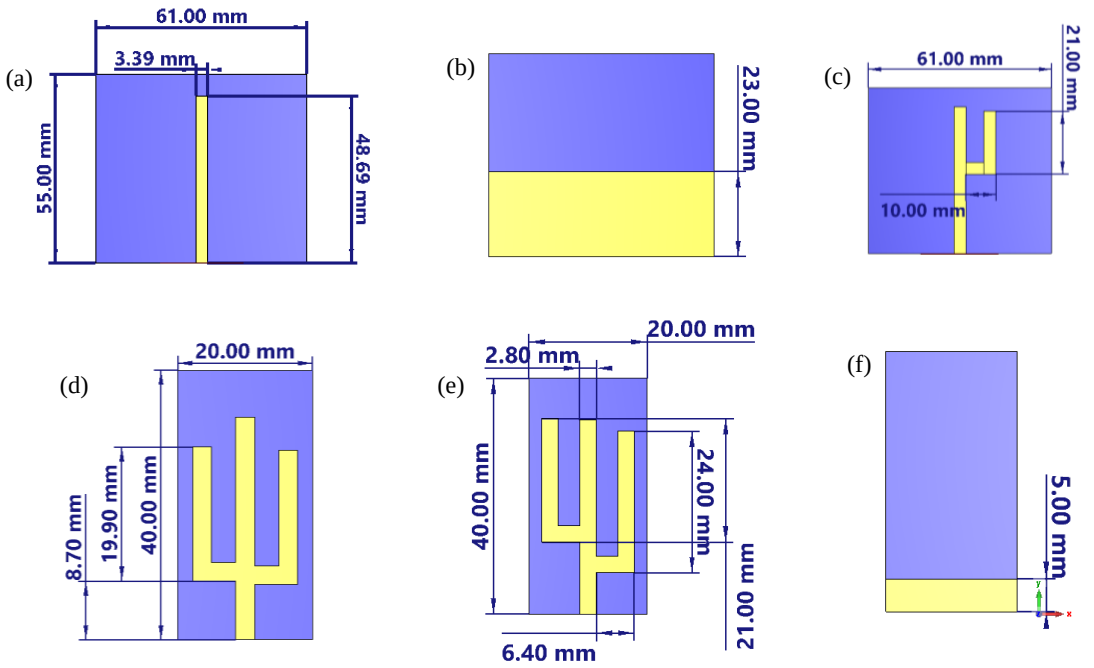

FIGURE 1. Design evolution of the proposed antenna: (a) Antenna-1 front. (b) Antenna-1 back. (c) Antenna-2. (d) Antenna-3. (e) Proposed antenna front. (f) Proposed antenna back.

negative gain values and reduced radiation efficiency on a human body phantom model.

The reported single-layer textile antennas [11–14] exhibit relatively large profiles and rely on additional structures or increased isolation from the human body to reduce the SAR levels. To overcome these limitations, a tri-arm-shaped jean-based monopole antenna is proposed and experimentally validated. To ensure the utility of the antenna for wearable applications, bending, crumpling, and on-body analyses were performed. The novelty of this work lies in achieving a compact, single-layer, low-profile, and low-cost antenna with inherently reduced SAR, thereby eliminating the need for complex structures, such as electromagnetic band gap, substrate-integrated waveguides, or metasurfaces.

2. ANTENNA DESIGN

Initially, a simple printed microstrip monopole of length $\lambda/4$ was designed, as shown in Figs. 1(a)–(b), for an operating frequency of 2.4 GHz in the Computer Simulation Technology (CST) Studio Suite [15]. The antenna was implemented on jeans with a dielectric constant of 1.9 and made up of cotton, polyester, and spandex with a thickness of 1.2 mm measured with the help of a vernier scale. The dielectric constant of the jean fabric was determined using the frequency resonance method detailed in [16]. The center frequency obtained for the stage-1 antenna was 2.7 GHz, with a reflection coefficient below −37 dB, as shown by the green curve in Fig. 2. In the next step, an L-shaped stub was added at the right side of the monopole, as depicted in Fig. 1(c), which resulted in dual-band resonance owing to the additional current path, with poor impedance matching and more reflections (refer to the blue curve in Fig. 2). The overall dimensions of the antenna were $61 \times 55\,\text{mm}^2$. Further, the antenna was miniaturized by adding another stub on the left side, as shown in Fig. 1(d), but the resonating frequency shifted from 2.5 to 2.8 GHz, as illustrated by the red curve in Fig. 2. The addition of the stub alters the electrical length of the antenna, creating an additional resonant path for the current, which results in a shift in the resonant frequency and dual-band resonance.

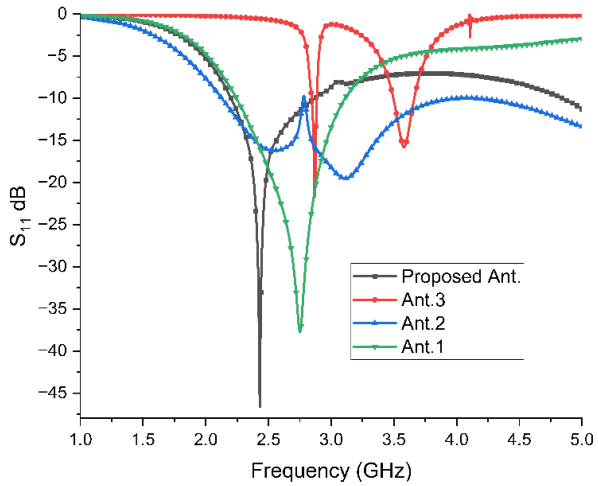

FIGURE 2. Reflection coefficient versus frequency graph of the evolutionary step and proposed antenna.

After a parametric study on the ground length, stub length, stub width, and stub position, the design of the proposed antenna was finalized. The proposed antenna has overall dimensions of $40 \times 20 \times 12\,\text{mm}^3$ as shown in Figs. 1(e)–(f). The antenna size was reduced by almost 50% compared to the stage-1

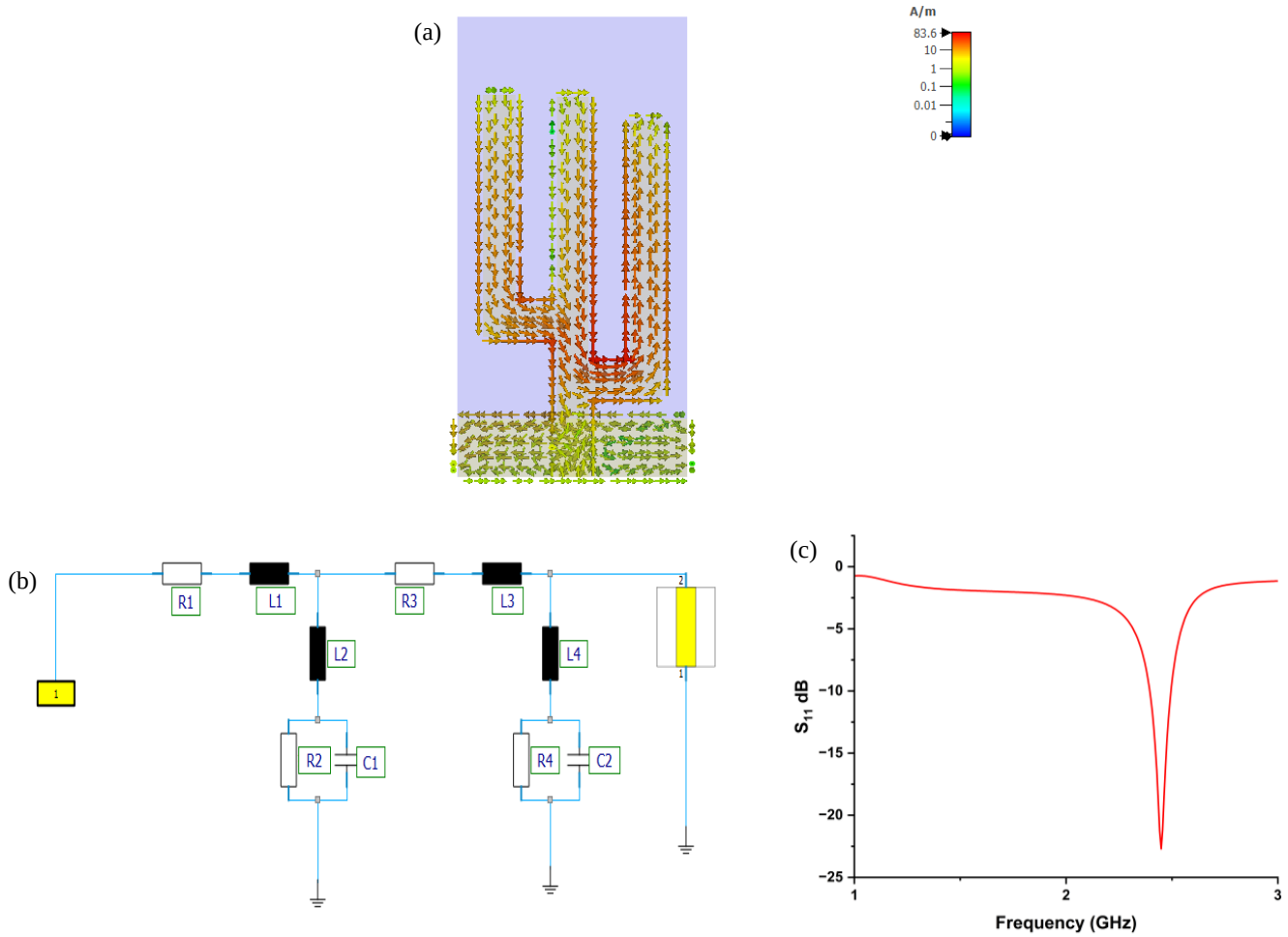

FIGURE 3. Proposed antenna. (a) Surface current distribution plot. (b) Equivalent circuit schematic diagram. (c) Return loss vs frequency graph for circuit model.

antenna, and the impedance bandwidth obtained was 580 MHz (23.86%). The proposed antenna covers a frequency band ranging from 2.20 to 2.78 GHz, as shown by the black curve in Fig. 2, with a center frequency of 2.43 GHz and a reflection coefficient below -46 dB.

The resonant behavior of the proposed antenna was studied using the surface current distribution graph, as illustrated in Fig. 3(a). The current density is higher at the feed points and at the edges of all three arms, indicating strong interactions and effective coupling between them. The graph confirms that the antenna is well-matched and radiates efficiently at the operating frequency.

The equivalent circuit model of the proposed antenna was designed using the Circuits and Systems Module in CST studio and is shown in Fig. 3(b). The two stubs were modelled as an impedance matching network, and the optimized distributed parameters were retrieved as $R1 = 3.61\,\Omega$, $L1 = 0.60$ nH, $L2 = 2.22$ nH, $R2 = 3.85$ kΩ, $C1 = 1.32$ pF, $R3 = 2.22\,\Omega$, $L3 = 0.31$ nH, $L4 = 2.12$ nH, $R4 = 5.89$ kΩ, $C2 = 3.23$ pF. The return loss graph for the circuit equivalent model is shown in Fig. 3(c), which shows the circuit model resonates at 2.4 GHz with S_{11} around -22 dB. The R-L-C component values may be further optimized for better impedance matching.

3. RESULTS AND DISCUSSION

The performance of the proposed tri-arm-shaped antenna was analyzed in free space, on a tissue-layer model, and validated through experimentation using metrics such as the reflection coefficient, gain, and radiation characteristics. An Agilent Technologies Vector Network Analyzer (VNA) N9925A was used to measure the antenna S-parameters, and VNA calibration was performed before testing to ensure error-free measurements.

3.1. Reflection Characteristics

The prototype of the tri-arm antenna fabricated on a jeans substrate using a cutter and fabric fusing tape is shown in Fig. 4(a). Fig. 4(b) shows the antenna testing using a VNA in free space, and Fig. 4(c) illustrates the antenna testing on the human forearm. The simulated and measured reflection coefficient results are shown in Fig. 5. The measured operating frequency in free space was observed at 2.44 GHz with S_{11} of -21.7 dB, which closely matched those obtained in the simulations.

The performance analysis of the antenna with respect to the body is crucial for ensuring safety and reliability for wearable applications. This analysis can be done using either the

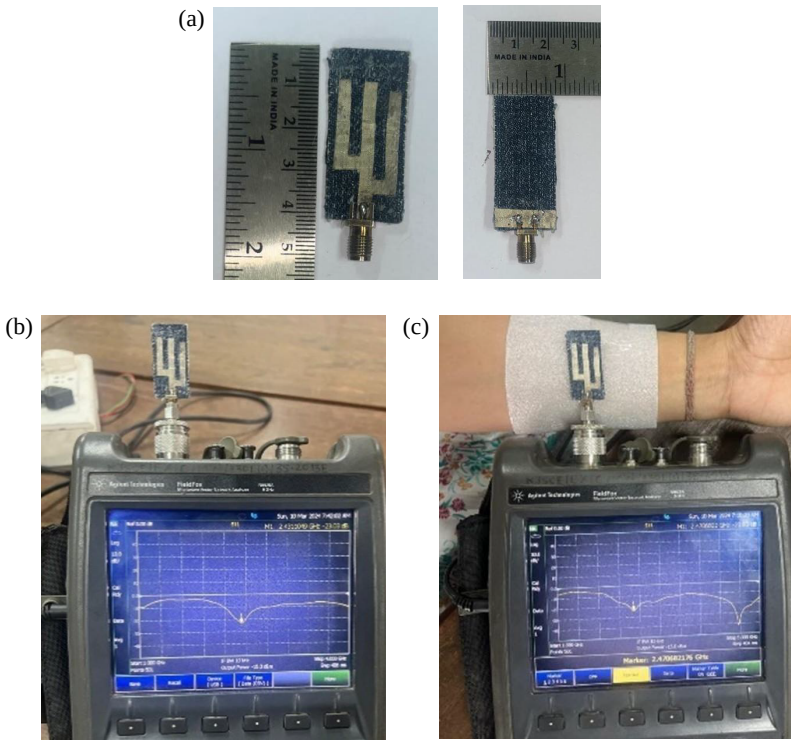

FIGURE 4. Proposed antenna. (a) Prototype showing the top and bottom sides. (b) Free-space measurement using VNA. (c) Measurement on the forearm.

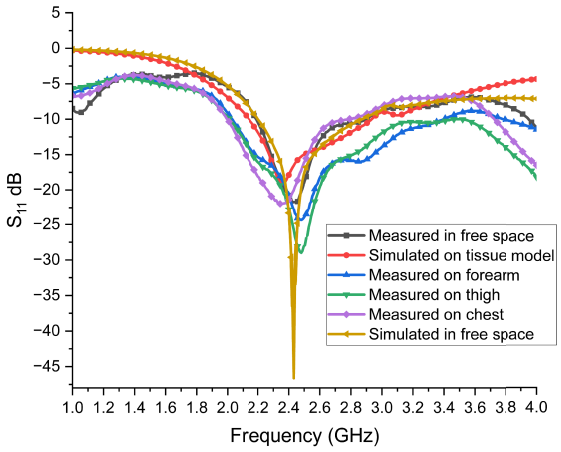

FIGURE 5. Return loss versus frequency plot of the proposed antenna in free space and on-body.

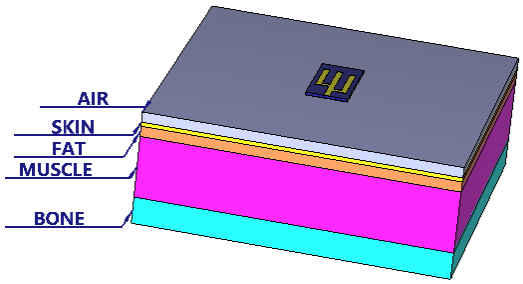

FIGURE 6. Proposed antenna positioned on tissue layer model.

TABLE 1. Multilayer tissue properties at 2.4 GHz [17].

Properties	Skin	Fat	Muscle	Bone
Epsilon	37.95	5.27	52.791	14
Loss tangent	0.2835	0.1938	0.2419	0.2524
Electric Cond. (S/m)	1.487	0.167	1.776	0.823
Density Rho (kg/m^3)	1001	900	1006	1008

voxel body models available in CST or the equivalent tissue layer mode. The proposed antenna performance was evaluated on a multilayer human tissue equivalent model consisting of skin (2 mm), fat (5 mm), muscle (30 mm), and bone (13 mm) of $100 \times 100\,\text{mm}^2$, as illustrated in Fig. 6. The antenna was isolated from the skin layer at a small distance of 5 mm represented by an air gap. The tissue properties at 2.4 GHz are mentioned in Table 1 [17].

The impedance bandwidth obtained on the tissue layer model was 780 MHz (2.14–2.92 GHz) with the resonant frequency at 2.36 GHz. The frequency was slightly shifted from free-space frequency, which is 2.43 GHz, but it effectively covered the ISM band. To validate the antenna performance for a wearable application, measurements were conducted on different body parts, such as the chest, forearm, and thigh. Due to human body loading, the effective dielectric constant of the patch is changed, and the antenna performance is slightly affected, resulting in resonant frequency shifts. When tested on the chest, the antenna resonated at 2.35 GHz with S_{11} around -22 dB, and the frequency shifted to 2.47 GHz when measured on the forearm

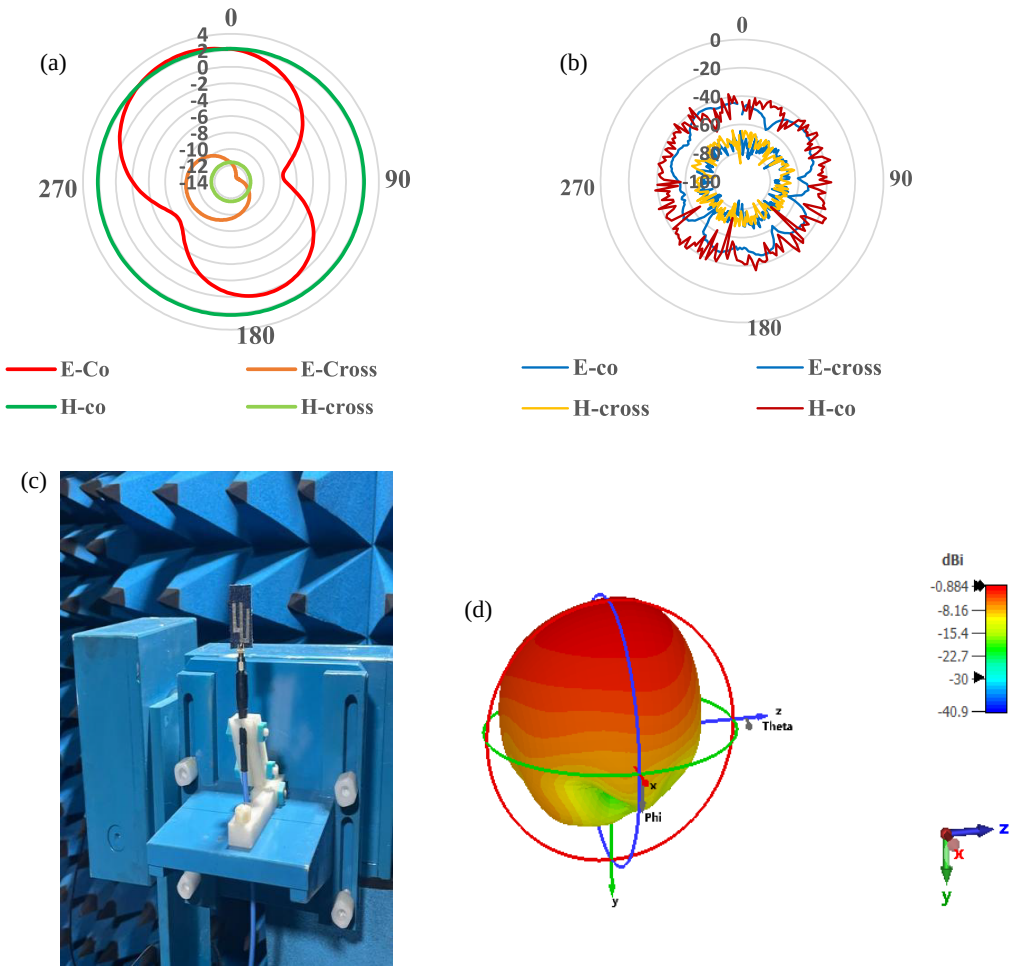

FIGURE 7. Radiation patterns, (a) simulated, (b) measured, (c) measurement setup in anechoic chamber, (d) radiation pattern on tissue layer model.

and thigh. In all the cases, the return loss values remained below -10 dB, and impedance bandwidth covered the ISM band.

3.2. Radiation Characteristics

The simulated radiation patterns of the proposed antenna, both co-polar and cross-polar, are presented in Fig. 7(a). The E-co pattern obtained was bidirectional, whereas the H-co radiation pattern was omnidirectional with good directivity values in both planes. The cross-polar components were approximately -15 dB, signifying good polarization purity. The realized gain of the antenna in free space was 1.9 dBi, whereas the measured gain was 1.6 dB, which is sufficient for body-centric communication applications.

The measured pattern plots are illustrated in Fig. 7(b). Fig. 7(c) shows the far-field radiation pattern measurement setup inside an anechoic chamber. The measured pattern in the H-plane was quite similar to the simulated pattern, but the E-plane pattern showed a null at a few points. The omnidirectional pattern in the azimuthal plane ensures reliable communication around the body.

Although there are minor fluctuations in the measured patterns, probably due to cable and connector losses, human applied pressure on the antenna during test setup, room temperature of the chamber, etc., the overall cross-polar discrimination is robust. The radiation pattern showing the gain simulated on the tissue layer model is depicted in Fig. 7(d). The power of the antenna is absorbed by lossy tissues, and the gain of the antenna is reduced. On the tissue model, the gain achieved was -0.884 dB. This gain is improved if the antenna is spaced 7 mm from the skin layer.

3.3. Bending and Crumpling Analysis

The fabric antennas are flexible and conform to the shape of the body; thus, bending and deformation are natural to occur with movements of the wearer. To ensure the reliability of the proposed antenna, a bending and crumpling analysis was conducted. The proposed antenna was bent along y-axis with three different bending diameters ($d = 50, 60, 70$ mm) to observe the effects on S-parameter. The selected diameter values serve as an approximation for the human forearm. The bending measurements were carried out using foam cylinders with diameters identical to simulation values. The bending along x-axis was not feasible due to the compact structure of the antenna, that is, the small width of the antenna and connector attachments; therefore, bending analysis was conducted along the y axis only. Moreover, the primary radiator undergoes significant

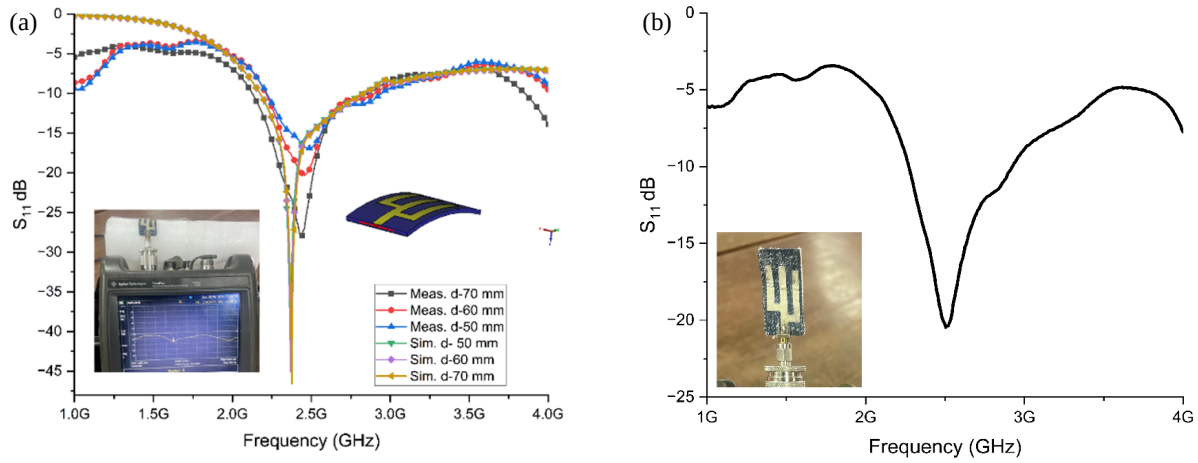

FIGURE 8. Return loss vs frequency graphs in case of deformations: (a) Bending. (b) Crumpling.

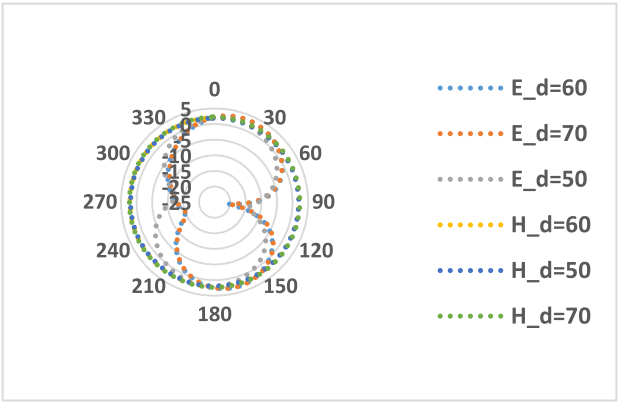

FIGURE 9. Effect of bending on antenna radiation pattern.

deformation along the y-axis, and the results are summarized in Fig. 8(a).

The proposed antenna showed excellent frequency stability under different bending scenarios. The resonance was around 2.45 GHz in all the bending cases. The simulated and measured results are well matched, validating the design's reliability for wearable applications. It was observed that with the decrease in bending diameter, the impedance matching is affected, and S_{11} shifts upwards. This shift was minor in the simulated scenario but noticeable in the experimentation study. The antenna was further crumpled and deformed under pressure to observe the changes in the reflection coefficient. Due to crumpling, there were random deformations across the radiating surface, leading to disturbances in the current distribution. As a result, the impedance matching was affected, leading to changes in return loss values. The proposed antenna resonated at 2.5 GHz with S_{11} around -20 dB in the case of crumpling as shown in Fig. 8(b). The proposed tri-arm antenna is resilient to major frequency detuning for both crumpling and bending cases.

Figure 9 illustrates the effect of bending on the antenna radiation pattern obtained in simulations. The radiation pattern in the H-plane was stable for different bending values. The main lobe magnitudes at 0° were 1.956 dBi, 2.088 dBi, and 2.292 dBi for bending diameters of 50, 60, and 70 mm, respectively. The radiation pattern in the E plane was moderately affected by decreasing the bending radius. The effect was more visible in the back lobe, and radiation pattern tilted slightly with different bending radii. Nevertheless, the overall radiation pattern performance is acceptable for wearable applications.

The measurement uncertainties may arise due to the fabrication tolerances of the textile material. Environmental factors, such as temperature, humidity, and the wearer's sweating, will affect the properties of textiles, resulting in variations in antenna performance. Furthermore, the measurement setup limitations arise, such as VNA calibration, connector and cable losses, which may introduce slight variations in measured results. The repeatability of the results may be affected by inconsistencies in the crumpling of the antenna.

3.4. SAR Evaluation

To ensure the safety of a person from antenna radiation, it is important to measure the SAR level. The upper limit of SAR is 1.6 W/kg, averaged over 1 g of tissue, and 2 W/kg, averaged over 10 g of tissue. SAR is the power absorbed per unit mass of the human body [2, 18]. The SAR value is related to the electromagnetic field and density of the tissue by the following equation:

$$S = \frac{\sigma |E|^2}{\rho} \tag{1}$$

where E denotes the electric field strength (V/m) in the tissue, σ the conductivity of the tissue (S/m), and ρ the density of the tissue (kg/m^3). The graph in Fig. 10(a) shows the SAR values calculated for the proposed antenna using different input powers (mW) for two measurement scenarios: 1 g and 10 g of tissue. The calculation was based on the IEEE C95.3 standard in the CST Studio. Both curves show an increase in SAR with increasing input power, indicating that SAR is dependent on the input power to the antenna. The peak SAR value achieved for the proposed antenna was 1.96 W/kg, averaged over 10 g of tissue, for an input power of 100 mW. The SAR value averaged over 1 g of tissue is 1.47 W/kg for 45 mW power, as shown in Fig. 10(b). Thus, the SAR values complied with the safety limits.

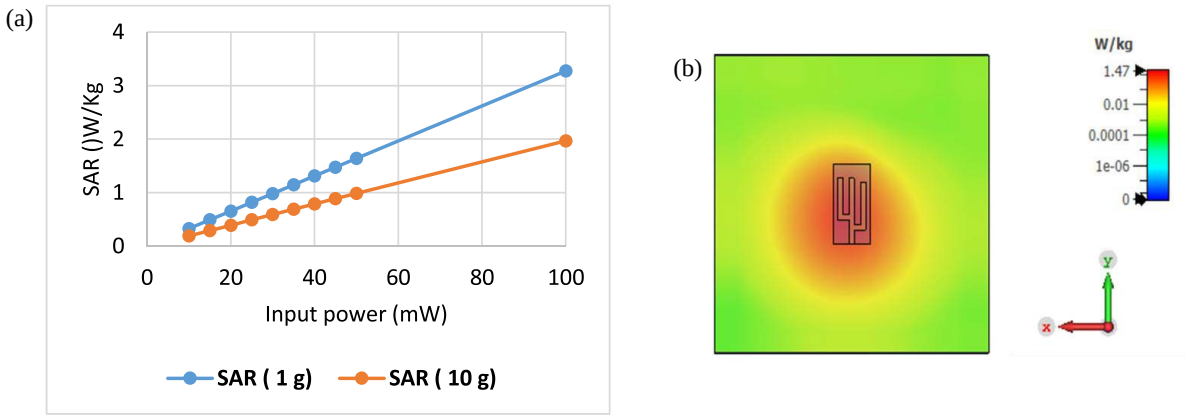

FIGURE 10. SAR evaluations: (a) Input power versus SAR. (b) SAR distribution over 1 g of tissue.

TABLE 2. Comparison between the proposed antenna and other textile antennas in free space reported in the literature.

Ref.	Frequency (GHz)	Bandwidth (MHz)	Efficiency (%)	SAR over 10 g tissue (W/kg)	Input Power for SAR evaluation (W)	Size of antenna (mm^3)	Isolation between antenna and body (mm)
[11]	2.45/5.48	60 @2.45	NR	0.258/0.185	0.5	$74 \times 82 \times 1$	NR
[13]	2.4	2857	70.96	0.0014	0.001	70×50	15
[19]	2.42	42	78	0.11	5	$80 \times 84 \times 2$	5
[20]	2.45/5.8	420	70.53/64	1.24/2.992	NR	$64.36 \times 76.96 \times 2.56$	12
[21]	2.45, 4.9 & 7.4	13.5% @2.45	86.13	0.068	0.001	$80 \times 80 \times 0.56$	10
[22]	2.45/3.32/3.93/5.8	3.7/5.7/5.85/9.8%	NR	0.11	1	$60 \times 60 \times 1.17$	5
This Work	**2.4**	**580 (23.86%)**	**82**	**1.47**	**0.1**	$\mathbf{40 \times 20 \times 1.2}$	**5**

NR: not reported

The proposed design was compared with similar works reported in the literature as illustrated in Table 2, and all the references were single-layer textile antenna designs to ensure a fair comparison. The proposed antenna has a higher impedance bandwidth and a more compact size than those of a few reported antennas. In [13], the isolation distance between the antenna and body was large (15 mm), along with a low input power of 1 mW for SAR evaluations. The proposed antenna was simulated for an input power of 100 mW and an isolation distance of 5 mm. In [20], the antenna isolation distance from the body was 12 mm, and the SAR levels were higher for the upper band. In [21], the authors obtained a low SAR value owing to the very low input power of 0.001 W. The proposed antenna is compact enough compared to all the reported works by a factor of approximately 40–50%.

4. CONCLUSION

A low-profile tri-arm monopole antenna on jeans is proposed for wearable applications. With an overall geometry of $40 \times 20 \times 1.2\ mm^3$, the proposed antenna demonstrated an efficiency of approximately 82%, and the gain achieved was 1.9 dBi. The measured free-space impedance bandwidth was 690 MHz, covering the ISM band with a measured gain of 1.6 dB. The bending and crumpling analyses showed that the antenna was resilient to major frequency detuning, making it a highly reliable candidate for wearable applications. The measurements conducted on different body locations, such as the forearm, chest, and thigh, demonstrated their positional robustness, maintaining an operating frequency of approximately 2.45 GHz. The peak SAR values obtained were 1.96 W/kg averaged over 10 g of tissue and 1.47 W/kg over 1 g of tissue. The proposed cost-effective and conformal jeans-based antenna stands out as a compact alternative with a single-layer configuration compared to metamaterial-based antennas.

ACKNOWLEDGEMENT

The authors would like to thank the Electronics and Telecommunication Department of K. J. Somaiya School of Engineering for providing laboratory facilities to conduct this research.

REFERENCES

[1] Hall, P. S. and Y. Hao, *Antennas and Propagation for Body-centric Wireless Communications*, Artech House, 2012.

[2] Ali, U., S. Ullah, B. Kamal, L. Matekovits, and A. Altaf, "Design, analysis and applications of wearable antennas: A review," *IEEE Access*, Vol. 11, 14 458–14 486, 2023.

[3] Paracha, K. N., S. K. A. Rahim, P. J. Soh, and M. Khalily, "Wearable antennas: A review of materials, structures, and innovative features for autonomous communication and sensing," *IEEE Access*, Vol. 7, 56 694–56 712, 2019.

[4] El Atrash, M., M. A. Abdalla, and H. M. Elhennawy, "A wearable dual-band low profile high gain low SAR antenna AMC-backed for WBAN applications," *IEEE Transactions on Antennas and Propagation*, Vol. 67, No. 10, 6378–6388, 2019.

[5] Gao, G., H. Meng, W. Geng, B. Zhang, Z. Dou, and B. Hu, "Design of a wide bandwidth and high gain wearable antenna based on nonuniform metasurface," *Microwave and Optical Technology Letters*, Vol. 63, No. 10, 2606–2613, 2021.

[6] Alemaryeen, A. and S. Noghanian, "On-body low-profile textile antenna with artificial magnetic conductor," *IEEE Transactions on Antennas and Propagation*, Vol. 67, No. 6, 3649–3656, 2019.

[7] Ashyap, A., R. Raad, F. Tubbal, W. A. Khan, and S. Abulgasem, "Comprehensive review of wearable antennas with flexible periodic structures for body-effect mitigation," *IEEE Access*, Vol. 13, 22 590–22 636, 2025.

[8] Varma, S., S. Sharma, M. John, R. Bharadwaj, A. Dhawan, and S. K. Koul, "Design and performance analysis of compact wearable textile antennas for IoT and body-centric communication applications," *International Journal of Antennas and Propagation*, Vol. 2021, No. 1, 7698765, 2021.

[9] Yan, S., V. Volskiy, and G. A. E. Vandenbosch, "Compact dual-band textile PIFA for 433-MHz/2.4-GHz ISM bands," *IEEE Antennas and Wireless Propagation Letters*, Vol. 16, 2436–2439, Jul. 2017.

[10] Arif, A., M. Zubair, M. Ali, M. U. Khan, and M. Q. Mehmood, "A compact, low-profile fractal antenna for wearable on-body WBAN applications," *IEEE Antennas and Wireless Propagation Letters*, Vol. 18, No. 5, 981–985, 2019.

[11] Thaiwirot, W., Y. Hengroemyat, T. Kaewthai, P. Akkaraekthalin, and S. Chalermwisutkul, "A dual-band low SAR microstrip patch antenna with jean substrate for WBAN applications," *International Journal of RF and Microwave Computer-Aided Engineering*, Vol. 2024, No. 1, 5076232, 2024.

[12] Kaur, H. and P. Chawla, "Design and performance analysis of wearable antenna for ISM band applications," *International Journal of Electronics*, Vol. 110, No. 6, 986–1005, 2023.

[13] Lin, X., Y. Chen, Z. Gong, B.-C. Seet, L. Huang, and Y. Lu, "Ultrawideband textile antenna for wearable microwave medical imaging applications," *IEEE Transactions on Antennas and Propagation*, Vol. 68, No. 6, 4238–4249, Jun. 2020.

[14] Ramasamy, K., B. A. Sapna, and M. Jayasheela, "A novel wearable monopole antenna with controlled SAR using metamaterial," *International Journal of Microwave and Wireless Technologies*, Vol. 15, No. 9, 1524–1536, 2023.

[15] Balanis, C. A., *Antenna Theory: Analysis and Design*, 3rd ed., John Wiley & Sons, Hoboken, USA, 2005.

[16] Sankaralingam, S. and B. Gupta, "Determination of dielectric constant of fabric materials and their use as substrates for design and development of antennas for wearable applications," *IEEE Transactions on Instrumentation and Measurement*, Vol. 59, No. 12, 3122–3130, Dec. 2010.

[17] Liang, R., Z. Liang, Y. Li, Y. Zhang, and S. Zheng, "A cylindrical conformal textile antenna with omnidirectional radiation pattern," *IEEE Access*, Vol. 12, 146 678–146 685, 2024.

[18] IEEE Standards Coordinating Committee, "IEEE standard for safety levels with respect to human exposure to radio frequency electromagnetic fields, 3 kHz to 300 GHz," IEEE C95.1-1991, 1992.

[19] Potey, P. M. and K. Tuckley, "Design of wearable textile antenna for low back radiation," *Journal of Electromagnetic Waves and Applications*, Vol. 34, No. 2, 235–245, 2020.

[20] Malar, K. A. and R. S. Ganesh, "Novel aperture coupled fractal antenna for Internet of wearable things (IoWT)," *Measurement: Sensors*, Vol. 24, 100533, 2022.

[21] Kaur, H. and P. Chawla, "Design and evaluation of a fractal wearable textile antenna for medical applications," *Wireless Personal Communications*, Vol. 128, No. 1, 683–699, 2023.

[22] Li, H., J. Du, X.-X. Yang, and S. Gao, "Low-profile all-textile multiband microstrip circular patch antenna for WBAN applications," *IEEE Antennas and Wireless Propagation Letters*, Vol. 21, No. 4, 779–783, 2022.